

### Charge-Transfer Mechanism for Electrophilic Aromatic Nitration and Nitrosation via the Convergence of (ab Initio) Molecular-Orbital and Marcus–Hush Theories with Experiments

Steven R. Gwaltney, Sergiy V. Rosokha, Martin Head-Gordon,\* and Jay K. Kochi\*

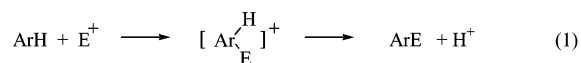
Contribution from the Department of Chemistry, University of California, Berkeley, California, 94720 and Department of Chemistry, University of Houston, Houston, Texas, 77 204

Received September 5, 2002; E-mail: jkochi@uh.edu

**Abstract:** The highly disparate rates of aromatic nitrosation and nitration, despite the very similar (electrophilic) properties of the active species:  $\text{NO}^+$  and  $\text{NO}_2^+$  in Chart 1, are quantitatively reconciled. First, the thorough mappings of the potential-energy surfaces by high level (ab initio) molecular-orbital methodologies involving extensive coupled-cluster CCSD(T)/6-31G\*\* optimizations establish the intervention of two reactive intermediates in nitration (Figure 8) but only one in nitrosation (Figure 7). Second, the same distinctive topologies involving double and single potential-energy minima (Figures 6 and 5) also emerge from the semiquantitative application of the Marcus–Hush theory to the transient spectral data. Such a striking convergence from quite different theoretical approaches indicates that the molecular-orbital and Marcus–Hush (potential-energy) surfaces are conceptually interchangeable. In the resultant charge-transfer mechanism, the bimolecular interactions of arene donors with both  $\text{NO}^+$  and  $\text{NO}_2^+$  spontaneously lead (barrierless) to  $\pi$ -complexes in which electron transfer is concurrent with complexation. Such a  $\pi$ -complex in nitration is rapidly converted to the  $\sigma$ -complex, whereas this Wheland adduct in nitrosation merely represents a high energy (transition-state) structure. Marcus–Hush analysis thus demonstrates how the strongly differentiated (arene) reactivities toward  $\text{NO}^+$  and  $\text{NO}_2^+$  can actually be exploited in the quantitative development of a single coherent (electron-transfer) mechanism for both aromatic nitrosation and nitration.

#### Introduction

Electrophilic aromatic substitutions are one of the best understood organic processes, and included in every (contemporary) organic textbook as the generic transformation:<sup>1,2</sup>



where the brackets identify the Wheland adduct as a high-energy intermediate that lies rather close to the rate-limiting transition state. As applied to the twin processes of aromatic nitration and nitrosation, the active electrophiles in eq 1 are thus  $\text{E}^+ = \text{NO}_2^+$  (nitronium) and  $\text{NO}^+$  (nitrosonium), respectively.<sup>3,4</sup> Because these cations are isolable as pure simple salts such as  $\text{NO}_2^+\text{SbCl}_6^-$  and  $\text{NO}^+\text{SbCl}_6^-$ , electrophilic aromatic nitration and nitrosation

#### Chart 1

Structure	$\text{NO}_2^+$	$\text{NO}_2^\bullet$	$\text{NO}^+$	$\text{NO}^\bullet$	Energy	$\text{NO}_2^+/\text{NO}_2^\bullet$	$\text{NO}^+/\text{NO}^\bullet$
d (N-O), Å	1.15	1.19	1.06	1.15	$E_{\text{red}}^\circ$ , V vs SCE	1.51	1.48
2θ (O-N-O), deg	180	134			IP, eV	9.60	9.27
$f_s$ , mdyne Å <sup>-1</sup>	17.4	11.0	23.9	15.9	$\lambda$ , kcal mol <sup>-1</sup>	140	69
$f_b$ , mdyne Å rad <sup>-2</sup>	0.69	1.58					

can both be examined directly as a bimolecular interaction in which only the static structures and physical properties of the cationic electrophiles such as those in Chart 1 provide the basis for evaluating their chemical reactivity. It is thus particularly noteworthy that (except for the inherent difference between diatomic and triatomic entities) the reductive changes of  $\text{NO}^+$  and  $\text{NO}_2^+$  in Chart 1 are strikingly similar – including their reversible potentials ( $E_{\text{red}}^\circ$  in solution) and ionization potentials (IP in the gas phase) which are essentially identical for both cations.<sup>5</sup> By contrast, the chemical reactivities of  $\text{NO}^+$  and  $\text{NO}_2^+$  toward various aromatic donors (ArH) are highly differentiated.

- (1) See, for example: (a) McMurry, J. *Organic Chemistry*, 3rd ed.; Brooks/Cole: Pacific Grove, California, 1992; pp 560 ff. (b) Carey, F. A. *Organic Chemistry*, 2nd ed.; McGraw-Hill: New York, 1992; pp 452 ff. (c) Roberts, J. D.; Caserio, M. C. *Basic Principles of Organic Chemistry*, 2nd ed.; Benjamin: Menlo Park, California, 1977; pp 1058 ff.
- (2) (a) Ingold, C. K. *Structure and Mechanism in Organic Chemistry*, 2nd ed.; Cornell Univ Press: Ithaca, 1986. (b) See also: Taylor, R. *Electrophilic Aromatic Substitution*, Wiley: New York, 1990. (c) De La Mare, P. B. D.; Ridd, J. H. *Aromatic Substitution. Nitration and Halogenation*; Butterworth: London, 1959. (d) Although electrophiles are most reactive as cationic species ( $\text{E}^+$ ), their neutral counterparts (E) are also to be included in any general formulation.

- (3) (a) Schofield, K. *Aromatic Nitration*, Cambridge University Press: Cambridge, 1980. (b) Olah, G. A.; Kuhn, S.; Mlinko, A. *J. Chem. Soc.* **1956**, 4257.
- (4) (a) Williams, D. L. H. *Nitrosation*, Cambridge: Cambridge University Press: 1988. (b) Bosch, E.; Kochi, J. K. *J. Org. Chem.* **1994**, *59*, 5573.

For example, the direct nitrations carried out with nitronium salts generally occur immediately upon mixing (even at low temperatures), whereas the corresponding nitrosation carried out with the related nitrosonium salt is too slow to be detected except for electron-rich arenes. In general,  $\text{NO}^+$  is estimated to be at least  $10^{14}$  times less effective than  $\text{NO}_2^+$ —which effects an encounter-controlled nitration of benzene.<sup>6</sup>

How can it be that a related pair of such active electrophiles as  $\text{NO}^+$  and  $\text{NO}_2^+$ , so similar in properties (Chart 1), can differ so markedly in arene reactivity? Clearly, the well-accepted mechanistic constructs as provided in textbooks are insufficient to reconcile such a glaring discrepancy, even to a qualitative degree. To address this mechanistic problem, we draw on two complementary theoretical approaches that specifically focus first on the quantum-mechanical description of the intermolecular potential-energy surfaces, and then on the interactions of the diabatic (reactants and products) states. For the former, we rigorously map out the bimolecular interactions of arene donors with  $\text{NO}^+$  and  $\text{NO}_2^+$  by employing first-principles electronic structure calculations to characterize the energy minima (and associated saddle points) along the reaction coordinates.<sup>7,8</sup> Because these molecular-orbital calculations are akin to accurate (numerical) experiments but provide only limited mechanistic insight, we turn to Marcus–Hush theory with important developments by Sutin,<sup>9</sup> in which adiabatic electron transfer can be rigorously developed from the non-interacting diabatic reactants (r) and final (f) states with the aid of only the reorganization energy ( $\lambda$ ), the intermolecular electronic coupling element ( $H_{DA}$ ), and the free-energy change ( $\Delta G_{ET}$ ). Most importantly, experimental data on the intermediates in the aromatic nitrosation are already (partially) available<sup>10</sup> in the form of molecular structures and electronic states (via X-ray crystallography and UV–vis spectra, respectively) of the intermolecular [1:1] complexes of various arenes with  $\text{NO}^+$  for ready comparison with those obtained via the ab initio molecular-orbital computations and those predicted by the Marcus–Hush treatment. In this paper, we show how the striking convergence of the molecular-orbital and Marcus–Hush potential-energy surfaces with experimental data provides unusual insight into the distinctive mechanism for (electrophilic) aromatic nitration<sup>11</sup> and nitrosation.

## Results

### I. Ab Initio Molecular-Orbital Mapping of the Potential-Energy Surfaces for Aromatic Nitrosation and Nitration.

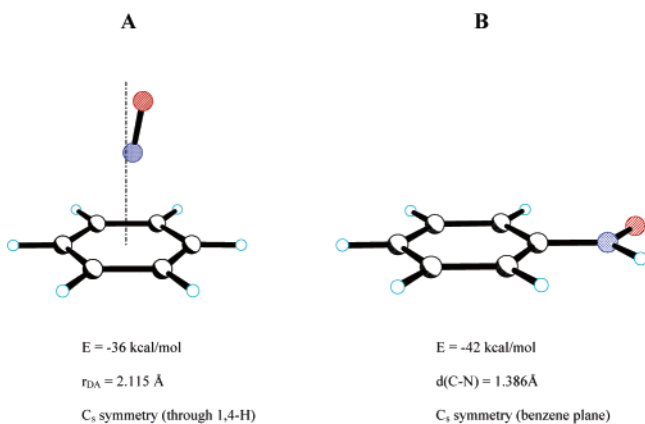
**Theoretical Methodology.** First-principles electronic structure calculations are performed by initial geometry (and energy) optimizations with second-order Møller–Plesset (MP2) theory<sup>12</sup>

- (5) (a) Reactivity of electrophiles ( $E^+$ ) according to the hard and soft acid–base formulation,<sup>b</sup>  $c$  resides in their reduction potential (electron affinity) or equivalently, the oxidation (ionization) potential of the reduced species E. (b) Pearson, R. G. *Chemical Hardness*; Wiley: New York, 1997. (c) *Hard and Soft Acid–Bases*; Pearson, R. G., Ed., Dowden, Hutchinson & Ross: Stroudsburg, PA, 1973.
- (6) Challis, B. C.; Higgins, R. J.; Lawson, A. J. *J. Chem. Soc. Perkin Trans 2*, **1972**, 1831.
- (7) See, for example: (a) Hehre, W. J.; Radom, L.; Pople, J.; Schleyer, P. N. R. *Ab Initio Molecular Orbital Theory*; Wiley: New York, 1986. (b) Jensen, F., *Introduction to Computational Chemistry*; Wiley: New York, 1999.
- (8) Head-Gordon, M. *J. Phys. Chem.* **1996**, *100*, 13 213.
- (9) (a) Marcus, R. A., Sutin, N. *Biochim. Biophys. Acta* **1985**, *811*, 265. (b) Sutin, N. *Prog. Inorg. Chem.*, **1983**, *30*, 441.
- (10) Kim, E. K.; Kochi, J. K. *J. Am. Chem. Soc.* **1991**, *113*, 4962.
- (11) For some alternative studies of electron-transfer nitration, see: (a) Perrin, C. L. *J. Am. Chem. Soc.* **1977**, *99*, 5516. (b) Lund, T.; Ebersson, L. *J. Chem. Soc., Perkin Trans. 2*, **1997**, 1435, and references therein.

and the 6-31G\*\* basis set,<sup>13</sup> as well as Kohn–Sham density functional theory (DFT) using the hybrid B3LYP functional<sup>14</sup> with the same basis set. All MP2 and DFT calculations are carried out with the Q-Chem electronic structure program.<sup>15a</sup> For the intermolecular closed-shell complexes of benzene and the diamagnetic acceptors  $\text{NO}^+$  and  $\text{NO}_2^+$ , the MP2 and B3LYP calculations (involving incomplete treatments of the electron-correlation effects) are carried out preliminarily with prior expectations of moderate accuracy. Therefore, to ensure significantly higher accuracy, we also perform high-level (CPU-intensive) coupled-cluster CCSD(T)<sup>16</sup> optimizations of all important (stationary and saddle) points by starting from their converged MP2 structures. We are confident that at this level of theory, the relative energies are accurate to within a few kcal mol<sup>-1</sup> of the exact results with this basis set,<sup>17</sup> although limitations of the latter may introduce some uncertainties. The CCSD(T) calculations are performed with the ACES II program.<sup>15b</sup> Solvation is treated as mainly being due to electrostatic effects by performing single point B3LYP computations within the Born and Onsager reaction field models<sup>18</sup> that employ spherical cavities at the centers of mass, with radii chosen to equal the maximum distance from the van der Waals radius of all atoms to this center.

**A. Intermolecular Interaction of Benzene and  $\text{NO}^+$ .** The relative energies and structural features of the stationary points (as energy minima) are summarized in Figure 1 for the intermolecular interaction of benzene and  $\text{NO}^+$ . Because most of these stationary points have been characterized and thoroughly discussed in the earlier report of Skokov and Wheeler using the B3LYP density functional with the 6-31G(d) basis set,<sup>19</sup> we shall keep our discussion of aromatic nitrosation brief, because our primary objective here is to set the stage for the aromatic nitration in the following section. As such, the initial encounter of benzene and  $\text{NO}^+$  leads to  $\pi$ -complex (Table 1), consistent with the previous calculation, which is computed to be 36 kcal mol<sup>-1</sup> below the diabatic reactants state ( $\text{C}_6\text{H}_6 + \text{NO}^+$ ) compared to the experimental estimate of  $44 \pm 5$  kcal

- (12) (a) Pople, J. A.; Binkley, J. S.; Seeger, R., *Int. J. Quantum Chem.* **1976**, *1*. (b) Head-Gordon, M. *Mol. Phys.* **1999**, *96*, 673.
- (13) (a) Hehre, W. J.; Ditchfield, R.; Pople, J. A., *J. Chem. Phys.* **1972**, *56*, 2257. (b) Hariharan, P. C.; Pople, J. A., *Mol. Phys.* **1974**, *27*, 209.
- (14) (a) Kohn, W.; Becke, A. D.; Parr, R. G., *J. Phys. Chem.* **1996**, *100*, 12 974. (b) Becke, A. D., *J. Chem. Phys.* **1993**, *98*, 5648.
- (15) (a) Kong, J.; White, C. A.; Krylov, A. I.; Sherrill, D.; Adamson, R. D.; Furlani, T. R.; Lee, M. S.; Lee, A. M.; Gwaltney, S. R.; Adams, T. R.; Ochsenfeld, C.; Gilbert, A. T. B.; Kedziora, G. S.; Rassolov, V. A.; Maurice, D. R.; Nair, N.; Shao, Y. H.; Besley, N. A.; Maslen, P. E.; Dombroski, J. P.; Daschel, H.; Zhang, W. M.; Korambath, P. P.; Baker, J.; Byrd, E. F. C.; Van Voorhis, T.; Oumi, M.; Hirata, S.; Hsu, C. P.; Ishikawa, N.; Florian, J.; Warshel, A.; Johnson, B. G.; Gill, P. M. W.; Head-Gordon, M.; Pople, J. A., *J. Comput. Chem.* **2000**, *21*, 1532. (b) Stanton, J. F.; Gauss, J.; Watts, J. D.; Nooijen, M.; Oliphant, N.; Perera, S. A.; Szalay, P. G.; Lauderdale, W. J.; Gwaltney, S. R.; Beck, S.; Balkova, A.; Bernholdt, D. E.; Baeck, K.-K.; Sekino, H.; Rozyczko, P.; Huber, C.; Bartlett, R. J. In: ACES II program as a product of the Quantum Theory Project, University of Florida. Integral packages included are VMOL (Almlöf and Taylor), VPROPS (Taylor) and a modified version of the ABACUS integral derivative package (Helgaker, Jensen, Olsen, Jorgensen and Taylor).
- (16) Raghavachari, K.; Trucks, G. W.; Pople, J. A.; Head-Gordon, M., *Chem. Phys. Lett.* **1989**, *157*, 479.
- (17) (a) Lee, T. J.; Scuseria, G. E. In *Quantum Mechanical Electronic Structure Calculations with Chemical Accuracy*; Langhoff, S. R., Ed.; Kluwer Academic: Dordrecht, 1995; Vol. 13. (b) The calculated energies include zero-point corrections, but are not corrected for basis set superposition errors (BSSE). Because the complexes are cationic, and the binding is very strong compared to typical intermolecular interactions, the BSSE effect should not be large. However, we hope that further computations in progress will shed additional light on this problem.
- (18) (a) Born, M. *Z. Phys.* **1920**, *1*, 45. (b) Onsager, L. *J. Am. Chem. Soc.* **1936**, *58*, 1486. See also: (c) Tomasi, J.; Cramer, C. J. et al. in ref 32 and Fukuzumi, S.; Kochi, J. K. *J. Am. Chem. Soc.* **1982**, *104*, 7599.
- (19) Skokov, S.; Wheeler, R. A. *J. Phys. Chem.* **1999**, *103*, 4261.



**Figure 1.** Molecular-orbital calculated energy minima corresponding to the [1:1]  $\pi$ -complex (left) and N-protonated nitrosobenzene product (right) from the intermolecular interaction of benzene and  $\text{NO}^+$ .<sup>56</sup>

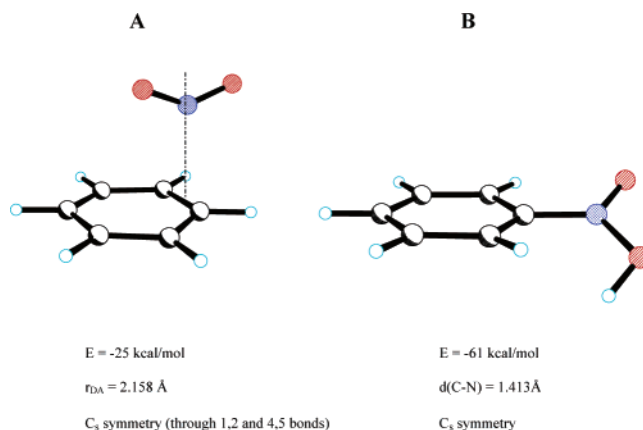
**Table 1.** Key Structural Parameters of the  $\pi$ -complexes of Benzene with  $\text{NO}^+$  and  $\text{NO}_2^+$  via Theory and Experiment

Electrophile (E)	E				
	d(N–O) <sup>a</sup>	d(C–C) <sup>b</sup>	r <sub>DA</sub> <sup>c</sup>	$\theta$ <sup>d</sup>	Z <sup>e</sup>
$\text{NO}^+$ (theor)	1.123	1.409	2.115	10	0.69
$\text{NO}^+$ (expt) <sup>g</sup>	1.09 ± 0.02	1.41 ± 0.01	2.12 ± 0.07	36 ± 15	0.74 ± 0.23
$\text{NO}_2^+$ (theor)	1.190 1.193	1.411	2.175	70 <sup>f</sup>	0.71
$\text{Br}_2$ (expt)	2.301 <sup>h</sup>	1.395	3.154	-	0.04 <sup>i</sup>

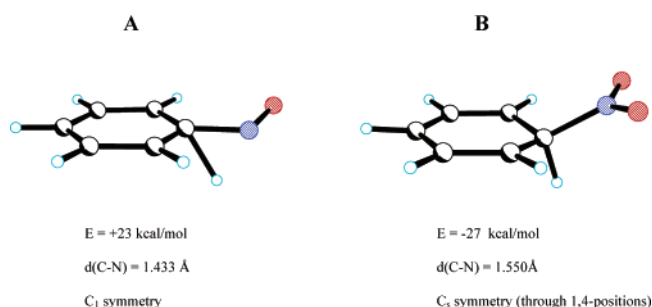
<sup>a</sup> N–O bond distance (Å). <sup>b</sup> Average C–C distance (Å). <sup>c</sup> Intermolecular (normal) separation of the electrophile from the benzene plane (Å). <sup>d</sup> Angle subtended by oxygen from the normal to the benzene plane. <sup>e</sup> Degree of charge transfer. <sup>f</sup>  $2\theta$  to represent the O–N–O angle. <sup>g</sup> Averages for  $[\text{ArH} \cdot \text{NO}]^+$  complexes, where ArH = TOL, o-XY, p-XY, MES, DUR, PMB or HMB (see structures in Table 3). <sup>h</sup> Dibromine bond distance (Å), from ref 26. <sup>i</sup> Based on  $H_{\text{DA}} = 0.6$  eV,  $\lambda = 2$  eV,  $\Delta E = 2.2$  V [estimated from UV–Vis spectral and X-ray crystallographic data for  $[\text{ArH} \cdot \text{Br}_2]$  complex and ( $E_{\text{ox}}^0 - E_{\text{red}}^0$ )].

$\text{mol}^{-1}$ .<sup>20,21</sup> As discussed in detail by Skokov and Wheeler, the  $\sigma$ -bonded Wheland structure is a saddle point rather than a true minimum in this dyad; and it represents a high-energy connection (transition state) between the  $\pi$ -complex and the product, calculated as the (N-protonated) nitrosobenzene. The latter lies 42 kcal  $\text{mol}^{-1}$  below the reactants in our calculations, versus the experimental estimate of  $52 \pm 7$  kcal  $\text{mol}^{-1}$ .<sup>22</sup>

**B. Intermolecular Interaction of Benzene and  $\text{NO}_2^+$ .** The relative energies and structural features of the stationary points in the  $\text{C}_6\text{H}_6/\text{NO}_2^+$  system that we have successfully optimized are presented in Figures 2 and 3B. Because these structures have not been previously described in theoretical reports,<sup>23–25</sup> we will discuss their characterization in more detail and contrast them with the  $\text{C}_6\text{H}_6/\text{NO}^+$  system outlined above. Thus, the initial



**Figure 2.** Molecular-orbital calculated energy minima corresponding to the [1:1]  $\pi$ -complex (left) and O-protonated nitrobenzene product (right) from the intermolecular interaction of benzene and  $\text{NO}_2^+$ .<sup>56</sup>

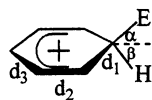


**Figure 3.** Optimized structures of the intermolecular  $\sigma$ -complexes of benzene with  $\text{NO}^+$  (A) and with  $\text{NO}_2^+$  (B) corresponding to the high-energy (saddle point) transition-state structure and the stable (energy minimum) adduct, respectively.<sup>56</sup>

encounter of  $\text{C}_6\text{H}_6$  with  $\text{NO}_2^+$  is also barrierless and leads directly to the intermolecular [1:1] complex some 25 kcal  $\text{mol}^{-1}$  below the diabatic reactants state. Although it is clearly  $\pi$ -bonding in nature, the resulting complex  $[\text{C}_6\text{H}_6 \cdot \text{NO}_2^+]$  exhibits a different geometry, and in addition attains only about two-thirds the stabilization energy of the analogous  $[\text{C}_6\text{H}_6 \cdot \text{NO}^+]$ . The key structural parameters of both  $\pi$ -complexes are compared in Table 1, together with those of a more traditional ( $\text{Br}_2$ ) structure established recently by X-ray crystallography.<sup>26</sup> It is particularly noteworthy that the  $\text{NO}_2^+$  acceptor binds to benzene directly above a single C–C center (at its midpoint); and this over-rim structure differs from the over-center structure of the  $\text{NO}^+$  analogue.<sup>27</sup> Such a  $\pi$ -complex has not been found in previous theoretical studies of the  $\text{C}_6\text{H}_6/\text{NO}_2^+$  system,<sup>28</sup> and we therefore thoroughly examine the optimization from a variety of initial conditions for consistent convergence to this energy minimum, including the initial condition that starts from benzene cation radical ( $\text{C}_6\text{H}_6^{\bullet+}$ ) and nitrogen dioxide ( $\text{NO}_2^{\bullet}$ ).<sup>29,30</sup> A

(20) (a) Reents, W. D.; Freiser, B. S. *J. Am. Chem. Soc.* **1980**, *102*, 271. (b) Reents, W. D.; Freiser, B. S. *J. Am. Chem. Soc.* **1981**, *103*, 2791. (c) In Skokov and Wheeler's calculation the  $\pi$ -complex minimum lies at  $-53$  kcal  $\text{mol}^{-1}$ .  
 (21) For comparison, the experimental (stabilization) energy in dichloromethane is  $-8$  kcal/mol (HMB).<sup>37</sup>  
 (22) (a) See Reents et al. in ref 20. (b) In Skokov and Wheeler's calculation the protonated product lies at  $-66$  kcal  $\text{mol}^{-1}$ .  
 (23) (a) Szabó, K. J.; Hörnfeldt, A.-B.; Gronowitz, S. *J. Am. Chem. Soc.* **1992**, *114*, 6827. (b) See also Tanaka, M.; Muro, E.; Ando, H.; Xu, Q.; Fujiwara, M.; Souma, Y.; Yamaguchi, Y. *J. Org. Chem.* **2000**, *65*, 2972.  
 (24) (a) Feng, J.; Zheng, X.; Zerner, M. C. *J. Org. Chem.* **1986**, *51*, 4531. (b) Politzer, P.; Jayasurya, K.; Sjöberg, P.; Laurence, P. R. *J. Am. Chem. Soc.* **1985**, *107*, 1174.  
 (25) (a) Peluso, A.; Del Re, G. *J. Phys. Chem.* **1996**, *100*, 5303. (b) Albulnia, A. R.; Borelli, R.; Peluso, A. *Theor. Chem. Acc.* **2000**, *104*, 218.

(26) Vasilyev A. V.; Lindeman, S. V.; Kochi, J. K. *New J. Chem.* **2002**, *26*, 582.  
 (27) The over-ring/over-center structural dichotomy in arene  $\pi$ -complexes has been noted in other electron donor/acceptor pairs. For a discussion, see: (b) Hubig, S. M.; Lindeman, S. V.; Kochi, J. K. *Coord. Chem. Rev.* **2000**, *200–202*, 831. (c) Fukin, G.; Lindeman, S. V.; Kochi, J. K. *J. Am. Chem. Soc.* **2002**, *124*, 8329. (d) See also Vasilyev et al. in ref 26.  
 (28) However, Peluso et al. in ref 25b (unlike previous investigators<sup>23, 24</sup>) seriously considered the importance of O–N–O bending in (their probable)  $\pi$ -complex formation.  
 (29) For the theoretical treatment of a pair of open-shell entities, compare: Jung, Y.; Head-Gordon, M. *J. Am. Chem. Soc.*, submitted for publication.  
 (30) Although this type of computational methodology cannot positively rule out the possibility of directly forming the Wheland intermediate from the diabatic reactants state (as previously concluded<sup>23</sup>), the burden of proof now lies in demonstrating that the  $\pi$ -complex is *not* an intermediate.

**Table 2.** Key Structural Parameters of Aromatic  $\sigma$ -complexes with Various (cationic) Electrophiles via Theory and Experiment<sup>a</sup>

Electrophile	$d_1$	$d_2$	$d_3$	$\alpha$	$\beta$
$\text{NO}_2^+$ (theor)	1.480	1.375	1.419	41	62
$\text{CH}_3^+$ (expt) <sup>b</sup>	1.493	1.375	1.423	55	55
$\text{Cl}^+$ (expt) <sup>c</sup>	1.493	1.369	1.431	56	50
$\text{Br}^+$ (expt) <sup>d</sup>	1.496	1.375	1.428	68	42
$\text{NO}^+$ (theor) <sup>e</sup>	1.492	1.372	1.422	52	52

<sup>a</sup> Bond distances in Å and angles in degree. <sup>b</sup> From ref 31a. <sup>c</sup> From ref 31b. <sup>d</sup> From ref 62. <sup>e</sup> Saddle-point structure (see text).

second stationary point is also found as a  $\sigma$ -bonded Wheland structure, which is calculated to be a significant minimum in the nitronium system, since it lies at 27 kcal mol<sup>-1</sup> below the diabatic reactants state ( $\text{C}_6\text{H}_6 + \text{NO}_2^+$ ). Comparison in Table 2 of the key structural parameters of such a  $\sigma$ -complex with those of similar cations established previously by X-ray crystallography,<sup>31</sup> provide the requisite confirmation as Wheland intermediates. This finding thus represents a second significant contrast between the nitrosonium and nitronium acceptors in which the  $\sigma$ -complex is calculated to be an energy minimum with  $\text{NO}_2^+$ , whereas it is a (high-energy) saddle point with  $\text{NO}^+$  (Figure 3). Finally, the hydrogen migration from carbon to oxygen restores the aromatic character, and the O-protonated nitrobenzene lies in a deep energy minimum of -61 kcal mol<sup>-1</sup>.

**C. Consideration of Solvent Effects.** The calculation of the stationary points for both  $\text{NO}^+$  and  $\text{NO}_2^+$  were performed in the vacuum in the first instance. Although the additional (proper) inclusion of molecular solvation effects is not rigorously possible at this juncture,<sup>8</sup> the leading electrostatic effects can be treated by reaction-field theory,<sup>32</sup> which we thus employ with the Born and Onsager approximation.<sup>18</sup> The results of the reaction-field calculation performed at the optimized minima for the  $\pi$ - and  $\sigma$ -complexes are summarized in Table S1 (see Supporting Information) for dielectric constants of 9 (dichloromethane) and 38 (acetonitrile). Barring the further treatment of solvation, we consider the effect of dichloromethane and acetonitrile on the relative energies to be reasonably modest and not to be of sufficient magnitude to preclude comparisons of the gas-phase calculations with the spectral data immediately following.

**II. Application of the Mulliken (Charge-Transfer) Formalism and Marcus–Hush Theory for Electron-Transfer from Arene Donors to  $\text{NO}^+$  and  $\text{NO}_2^+$ . Theoretical Background.** The intermolecular interaction of aromatic donors (D) to various electron acceptors including:  $\text{A} = \text{NO}^+$ ,  $\text{NO}_2^+$ , etc. results in characteristic (UV–vis) absorption bands diagnostic of the very rapid formation of charge-transfer complexes.<sup>10</sup> Such intermolecular [1:1] complexes in the general context of Mulliken theory<sup>33</sup> are generated by the linear combination of the principal van der Waals ( $\psi_{\text{D,A}}$ ) and dative ( $\psi_{\text{D}^+\text{A}^-}$ ) states; so that the ground-state ( $\Psi_{\text{GS}}$ ) and excited-state ( $\Psi_{\text{ES}}$ ) wave

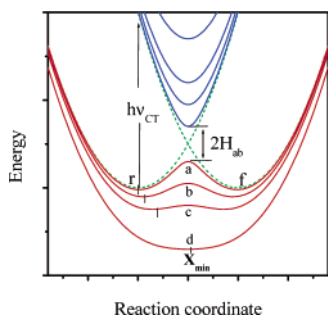
functions in the charge-transfer model can be expressed as<sup>34–36</sup>

$$\Psi_{\text{GS}} = c_a \psi_{\text{D,A}} + c_b \psi_{\text{D}^+\text{A}^-} \text{ and } \Psi_{\text{ES}} = c_b \psi_{\text{D,A}} - c_a \psi_{\text{D}^+\text{A}^-} \quad (2)$$

The energies of ground and excited states  $E_{\text{GS}}$  and  $E_{\text{ES}}$  from solving the two-state secular determinant (by application of the variational method) can be expressed in terms of the Coulomb integrals:  $\int \psi_{\text{D,A}} \mathcal{H} \psi_{\text{D,A}}$  and  $\int \psi_{\text{D}^+\text{A}^-} \mathcal{H} \psi_{\text{D}^+\text{A}^-}$  (representing the energies  $\epsilon_{\text{D,A}}$  and  $\epsilon_{\text{D}^+\text{A}^-}$  of the van der Waals and dative states, respectively), and the resonance integral:  $\int \psi_{\text{D,A}} \mathcal{H} \psi_{\text{D}^+\text{A}^-} = H_{\text{DA}}$  (electronic coupling matrix element).<sup>35–39</sup> The energy gap is as follows:  $\Delta = \epsilon_{\text{D}^+\text{A}^-} - \epsilon_{\text{D,A}}$ . The normalized mixing coefficients determine the electron-density distribution between the donor and acceptor moieties in the complex (energy minimum) and are related to the electronic coupling element as:<sup>36</sup>  $c_a c_b = H_{\text{DA}} / (E_{\text{ES}} - E_{\text{GS}})$ , and to the degree of charge transfer defined as:  $Z = 2c_b^2$  (i.e., evaluation of  $Z$  leads to estimation of  $H_{\text{DA}}$ ).<sup>35,37,40</sup> The charge-transfer energy ( $\nu_{\text{CT}}$ ) of

- (34) (a) Equations 2 represent the valence-bond formulation of the charge-transfer complex, but the molecular-orbital formulation is comparable. [See: (b) Flurry, R. L. *J. Phys. Chem.* **1965**, *69*, 1927. (c) Flurry, R. L. *J. Phys. Chem.* **1969**, *73*, 2111. (d) Flurry, R. L. *J. Phys. Chem.* **1969**, *73*, 2787.] (e) The mixing coefficients in eqs 2 are constrained to the normalized:  $c_a^2 + c_b^2 = 1$ .
- (35) Rosokha, S. V.; Kochi, J. K. *New J. Chem.* **2002**, *26*, 851.
- (36) (a) Brunschwig, B. S.; Sutin, N. *Coord. Chem. Rev.* **1999**, *187*, 233. (b) Creutz, C.; Newton, M. D.; Sutin, N. *J. Photochem. Photobiol. A: Chem.* **1994**, *82*, 47. (c) Brunschwig, B. S.; Sutin, N. In *Electron Transfer in Chemistry*; V. Balzani, Ed.; Wiley: New York, 2001; Vol. 2., p 583.
- (37) (a) Rosokha, S. V.; Kochi, J. K. *J. Am. Chem. Soc.* **2001**, *123*, 8985. (b) The direct relationship between the experimental and theoretical measures of  $Z$  are described herein.
- (38) Mulliken theory represents the energies of ground and excited states as:<sup>36</sup>  $E_{\text{GS}} = (\epsilon_{\text{D,A}} + \epsilon_{\text{D}^+\text{A}^-})/2 - (\Delta^2 + 4H_{\text{DA}}^2)^{1/2}/2$  and  $E_{\text{ES}} = (\epsilon_{\text{D,A}} + \epsilon_{\text{D}^+\text{A}^-})/2 + (\Delta^2 + 4H_{\text{DA}}^2)^{1/2}/2$ . According to Marcus,<sup>41</sup> the energies of the reactants and final diabatic states versus the reaction coordinate ( $X$  taken as the nuclear coordinate) are represented by parabolas with the coefficients equal to the reorganization energy, i.e.,  $\epsilon_{\text{DA}} = \lambda X^2$  and  $\epsilon_{\text{D}^+\text{A}^-} = \lambda(1 - X)^2 + \Delta G^\circ$ . Substitution yields the adiabatic states as follows:  $E_{\text{GS}} = [\lambda(2X^2 - 2X + 1) + \Delta G^\circ]/2 - \{[\lambda(2X - 1) - \Delta G^\circ]^2 + 4H_{\text{DA}}^2\}^{1/2}/2$  and  $E_{\text{ES}} = [\lambda(2X^2 - 2X + 1) + \Delta G^\circ]/2 + \{[\lambda(2X - 1) - \Delta G^\circ]^2 + 4H_{\text{DA}}^2\}^{1/2}/2$ , the graphical representation of which are shown as the solid curves in Figure 4 for isergonic systems with  $\Delta G^\circ = 0$ .
- (39) (a) Hush, N. S. *Z. Electrochem.* **1957**, *61*, 734. (b) Hush, N. S. *Trans. Faraday Soc.* **1961**, *57*, 557. (c) Hush, N. S. *Prog. Inorg. Chem.* **1967**, *8*, 391. (d) Hush, N. S. *Electrochim. Acta.* **1968**, *13*, 1005. (e) Using the Mulliken formalism, Hush showed<sup>39c,d</sup> that the electronic coupling element is related to characteristics of electronic transition maximum,  $\nu_{\text{CT}}$  (cm<sup>-1</sup>), width  $\Delta\nu_{1/2}$  (cm<sup>-1</sup>), and extinction coefficient  $\epsilon_{\text{max}}$  (M<sup>-1</sup>cm<sup>-1</sup>) as eq 3, where  $r_{\text{DA}}$  is the donor/acceptor separation (Å) in complex.
- (40) (a) In the two-state model, the quantitative relationship for the degree of charge transfer in the nitrosonium and nitronium complexes is:  $Z = 2c_b^2 = 1 - [1 - (2H_{\text{DA}}/\nu_{\text{CT}})^2]^{1/2}$  as described by Rosokha et al. in ref 35. Thus, the electronic coupling element can be calculated with the aid of this expression using the UV–vis and IR data to evaluate the parameters  $\nu_{\text{CT}}$  and  $Z$ , respectively, because the rearrangement of this equation yields:  $H_{\text{DA}} = \nu_{\text{CT}}(1 - (1 - Z)^2)^{0.5}/2$ . (b) It is important to note that the  $H_{\text{DA}}$  values in Table 3 are essentially the same (within 5%) as those previously evaluated via the simplified molecular-orbital model.<sup>37a</sup> By comparison, the values of  $H_{\text{DA}}$  calculated via the Mulliken–Hush methodology (eq 3) are consistently lower (~40%)<sup>35</sup> than those in Table 3 probably owing to the uncertainty in the  $r_{\text{DA}}$  parameter in these strongly coupled systems. (c) From the analytical expression of the adiabatic ground state,<sup>38</sup> the minimum (i.e.,  $dE_{\text{GS}}/dX = 0$ ) for  $\lambda_{\text{CE}} = 4$  eV and  $Z = 0.71$  leads to  $H_{\text{DA}} \approx 1.7$  eV (d) The application of the two-state model to  $[\text{ArH}, \text{NO}]^+$  as a Class III system may seem inappropriate in view of the strong donor/acceptor interaction extant with substantial orbital overlap. However, it is important to emphasize that we have employed three separate and more or less independent methodologies for the evaluation of  $H_{\text{DA}}$  that lead to the same results<sup>40a,b</sup> and such a consistency indicates that calculations based on the two-state model are applicable to  $[\text{ArH}, \text{NO}]^+$ . Most importantly, these results coincide with the extensive experimental data that establish a *single potential-energy minimum* for which: (1) detailed X-ray crystallography of the structural ( $\text{NO}^+$ , ArH) changes; (2) infrared analysis of the N–O stretching frequencies, (3) <sup>13</sup>C NMR spectroscopy of the complexed arene; (4) spectral analysis of the electronic (CT) transitions establish the unique character of the strong  $\text{NO}^+$ /ArH bonding symptomatic of a Class III complex. We thus interpret these narrowly converged results to indicate that the two-state model provides a consistently reasonable and accurate description of the ArH/ $\text{NO}^+$  interaction.

- (31) (a) Borodkin, G. I.; Nagi, S. M.; Gatilov, Y. V.; Sharikov, M. M.; Rybalvo, T. V.; Shubin, V. G. *Zh. Org. Chim.* **1992**, *28*, 1806. (b) Nugent, W. A. *J. Org. Chem.* **1980**, *45*, 4534. For X-ray crystallography of some relevant arene  $\sigma$ -complexes, see: Hubig et al. in ref 57.
- (32) See, for example: (a) Tomasi, J.; Persico, M. *Chem. Rev.* **1994**, *94*, 2027. (b) Cramer, C. J.; Truhlar, D. G. *Chem. Rev.* **1999**, *99*, 21 610.
- (33) (a) Mulliken, R. S. *J. Am. Chem. Soc.* **1952**, *74*, 811. (b) Mulliken, R. S.; Person, W. B. *Molecular Complexes*; Wiley: New York, 1969.



**Figure 4.** Generalized (cross-sectional) cuts of the potential-energy surfaces along the reaction coordinate for an adiabatic electron transfer ( $\Delta G^0 = 0^{42}$ ) with the ground states represented in red and the corresponding excited states in blue. The electronic coupling increases from the diabatic reactants (r) and final (f) states (green dotted lines) with  $H_{DA}/\lambda = 0$  to various adiabatic states (red curves) with  $H_{DA}/\lambda = 0.10$  (a), 0.22 (b), 0.35 (c), and 0.60 (d).

the intermolecular complex corresponds to the optical transition:  $\Psi_{GS} \rightarrow \Psi_{ES}$ , and is given by:  $\nu_{CT} = (\Delta^2 + 4H_{DA}^2)^{1/2}$ ; and coupling element can be evaluated from the spectral characteristics of complex via Mulliken–Hush expression (eq 3).<sup>36,39</sup>

$$H_{DA} = 0.0206(\nu_{CT} \Delta\nu_{1/2} \epsilon_{CT})^{1/2}/r_{DA} \quad (3)$$

Although the primary focus of the Mulliken theory is on the static properties of CT complexes, the combination of the Mulliken formalism with the Marcus (quadratic) representation of the diabatic reactants (r  $\equiv \psi_{D,A}$ ) and final (f  $\equiv \psi_{D+A^-}$ ) states (dashed curves in Figure 4)<sup>38</sup> allows the energy profile for the redox dynamics to be constructed.<sup>38,41,42</sup> The lower (solid) curves represent the cross-sections of the potential-energy surfaces for thermal (adiabatic) electron transfer which are separated from the corresponding excited-state surfaces by the varying magnitudes of the electronic coupling element ( $2H_{DA}$ ).

**A. Potential Energy Diagram for Arene Interaction with  $\text{NO}^+$  via Electron Transfer.** Immediately upon the addition of an arene to a colorless  $\text{NO}^+$  solution, intermolecular charge-transfer complexes were observed as reversible bright yellow to red colorations, i.e.



and spectroscopic examinations revealed a series of ArH-dependent absorption bands that obeyed the Mulliken correlation (Table 3).<sup>35,37</sup> The slow subsequent reactions leading from eq 4 to aromatic nitrosation<sup>4b</sup> allowed the metastable intermediates to be isolated and structurally confirmed as [1:1] complexes in Table 1 (second entry), in which the intermolecular separation of the  $\text{NO}^+$  moiety from the aromatic plane of  $r_{DA} \approx 2.1 \text{ \AA}$

was significantly closer than the sum of the van der Waals radii of  $3.25 \text{ \AA}$ . Most importantly, the  $\text{NO}^+$  complexation also resulted in an expansion of the aromatic (C–C) bond length to  $1.41 \text{ \AA}$  (average) and approached that of the oxidized aromatic cation radical ( $\text{ArH}^{+\bullet}$ ); as well as the lengthening of the N–O bond that was closer to that of the reduced  $\text{NO}^\bullet$  ( $1.15 \text{ \AA}$ ) than that of the uncomplexed  $\text{NO}^+$  ( $1.06 \text{ \AA}$ ). The latter was independently verified by IR spectroscopy showing the stretching frequency ( $\nu_{\text{NO}}$  in Table 3) to approximate that of nitric oxide ( $1876 \text{ cm}^{-1}$ ) compared to the uncomplexed nitrosonium ( $2272 \text{ cm}^{-1}$ ), and confirmed by  $^{13}\text{C}$  NMR spectroscopy.<sup>10</sup> Thus, all the experimental data were consistent; and they showed the arene/ $\text{NO}^+$  complexes to represent the close association and extensive charge delocalization between the arene and  $\text{NO}^+$  moieties. The experimental degree of charge-transfer Z evaluated from the N–O stretching frequencies (IR) is included in Table 3.<sup>35,37a</sup> The electronic character of such an intermolecular complex was elucidated by the Mulliken–Hush analysis of the charge-transfer absorption bands.<sup>35,40b</sup>

The reversible association of arene donors with  $\text{NO}^+$  (as described in eq 4) was followed by a dissociative electron-transfer step,<sup>37</sup> i.e., eq 5



Accordingly, the overall driving force for the electron transfer was given by

$$\Delta G_{ET} = \mathcal{F}(E_{ox}^\circ - E_{red}^\circ)$$

where  $\mathcal{F}$  is the Faraday constant,  $E_{ox}^\circ$  represents the oxidation potential of the arene (Table 3) and  $E_{red}^\circ$  is the reduction potential of  $\text{NO}^+$  (Chart 1).

Sutin's development of the Marcus–Hush formulation<sup>9,36</sup> specifically focuses on the electronic coupling element, and he considers two major mechanistic categories based on the Robin–Day classification,<sup>43</sup> in which the limits of the electronic coupling element are as follows

$$H_{DA} > \lambda_{CE}/2 \quad (\text{Class III}) \quad (6)$$

$$H_{DA} < \lambda_{CE}/2 \quad (\text{Class II})^{44} \quad (7)$$

where  $\lambda_{CE}$  is the Marcus reorganization energy (intrinsic barrier) for the cross-exchange such as that in eq 5.<sup>45</sup> Within this context, the value of  $\lambda_{CE}$  was obtained from their self-exchanges: (ArH

(41) (a) Marcus, R. A. *J. Phys. Chem.* **1963**, *67*, 853. (b) Marcus, R. A. *J. Chem. Phys.* **1965**, *43*, 679.


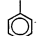
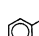
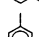
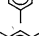

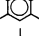
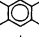
(42) (a) We have chosen to illustrate the Marcus–Hush analysis in Figures 4–6 ( $\Delta G_{ET}^0 = 0$ ) to allow the direct comparison with the quantum-mechanical (MO) modeling shown in Figures 7 and 8, which are based on (nearly) isergonic processes. [Note that such systems allow the effects of  $\lambda$  and  $H_{DA}$  on the potential-energy profile to be clearly identified in the absence of a driving-force component.<sup>70</sup>] (b) In the gas phase, this process corresponds to:  $\text{C}_6\text{H}_6 + \text{NO}^+/\text{NO}_2^+ \rightleftharpoons \text{C}_6\text{H}_6^{+\bullet} + \text{NO}^\bullet/\text{NO}_2^\bullet$  and (c) in solution it is:  $\text{C}_6(\text{CH}_3)_6 + \text{NO}^+/\text{NO}_2^+ \rightleftharpoons \text{C}_6(\text{CH}_3)_6^{+\bullet} + \text{NO}^\bullet/\text{NO}_2^\bullet$ , as described by Rosokha et al. in ref 37. (d) For aromatic nitration: because the SC can transform directly to the  $\sigma$ -adduct or other products without the intervention of the diabatic (radical pair) state as in Figure 8, the electron-transfer mechanism is not necessarily obviated by forbiddingly high endergonic driving forces ( $-\Delta G_{ET}$ ).

(43) (a) Robin, M. B.; Day, P. *Adv. Inorg. Chem. Radiochem.* **1967**, *10*, 247. (b) Although this classification is based on symmetrical mixed-valence complexes, Sutin showed that it is applicable to nonsymmetrical systems,<sup>36a</sup> and we believe that it is also applicable to intermolecular complexes of type described in this study.

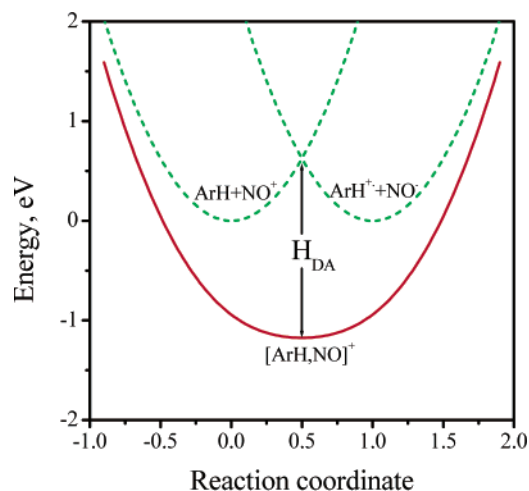
(44) For Class II,  $H_{DA} > 0 \text{ cm}^{-1}$ .

(45) (a) The reorganization energies for the cross-exchange reaction (CE) obtained from the reorganization energy of the self-exchange for  $\text{ArH}/\text{ArH}^{+\bullet}$ <sup>46a</sup> and for  $\text{NO}^+/\text{NO}^\bullet$ <sup>46b</sup> as:  $\lambda_{CE} = (\lambda_{\text{NO}} + \lambda_{\text{ArH}})/2$  lie in the range: 2.4–2.6 eV. (b) The validity of these estimates was independently examined by an alternative procedure based on the spectral/electrochemical data as:  $\lambda_{CE} = (\Delta - \Delta G_{ET})/(1 - 2X)$  which follows from analysis made by Brunschwig et al.<sup>36c</sup> (and the terms can be identified in their eq 3b). Typical values evaluated by this procedure for individual arene donors are: benzene (1.9 eV), toluene (2.5), *p*-xylene (2.6 eV) mesitylene (3.3 eV); but the evaluation of the better donors (approaching the isergonic region) suffers from the increasing inaccuracy of the denominator owing to:  $(1 - 2X) \rightarrow 0$ .

**Table 3.** Oxidation Potentials of Aromatic Donors ( $E^{\circ}_{\text{ox}}$ ), the Spectral Characteristics of the Charge-transfer Band ( $\nu_{\text{CT}}$ ,  $\Delta\nu_{1/2}$  and  $\epsilon$ ), Electronic Coupling Elements ( $H_{\text{DA}}$ ), and Degree of Charge-transfer ( $Z$ ) in Their Complexes with the Nitrosonium Acceptor

Arene donor	$E^{\circ}_{\text{ox}}$ <sup>a</sup>	$\nu_{\text{CT}}$ <sup>b</sup>	$\Delta\nu_{1/2}$ <sup>b</sup>	$\epsilon$ <sup>b</sup>	$\nu_{\text{NO}}$ <sup>a</sup>	$Z$	$H_{\text{DA}}$ <sup>c</sup>	eV
BEN 	2.70	29.8	6.0	1.6	2075	0.52	1.62	
TOL 	2.42	29.6	6.5	3.5	2030	0.61	1.69	
o-XY 	2.13	29.8	6.1	3.5	2000	0.69	1.76	
p-XY 	2.06	30.2	6.8	4.0	1998	0.70	1.78	
MES 	2.11	29.5	5.9	5.8	1964	0.75	1.77	
DUR 	1.83	30.3	5.9	7.0	1933	0.86	1.86	
PMB 	1.75	30.1	6.0	8.1	1907	0.92	1.86	
HMB 	1.62	30.1	6.0	8.0	1885	0.97	1.87	

<sup>a</sup> Ref 10. <sup>b</sup> Ref 35. <sup>c</sup> See footnote 40a.



**Figure 5.** Potential-energy diagram (single minimum) for electron-transfer in  $\text{NO}^+/\text{ArH}$  dyads with  $\lambda = 2.5$  eV and  $\Delta G^\circ = 0$  eV. Dashed green lines represent the diabatic (noninteracting) initial (separated reactants) state and the final (separated products) state. Bold solid (red) curve represents the adiabatic state when  $H_{\text{DA}} = 1.8$  eV (drawn to scale).

$\rightleftharpoons \text{ArH}^+ + \text{NO}^+ \rightleftharpoons \text{NO}^*$ ), based on  $\lambda_{\text{ArH}} = 40\text{--}50$  kcal mol<sup>-1</sup> and  $\lambda_{\text{NO}} = 69$  kcal mol<sup>-1</sup>, respectively.<sup>46</sup>

To evaluate the electronic coupling element pertinent to the  $[\text{ArH}, \text{NO}]^+$  complexes, we utilize the quantitative relationship between the charge-transfer absorption and the degree of charge transfer.<sup>40</sup> The values of  $H_{\text{DA}}$  obtained by this procedure are listed in Table 3 (column 9). Their magnitudes:  $H_{\text{DA}} = 1.6\text{--}1.8$  eV are substantially greater than  $\lambda_{\text{CE}}/2 = 1.2\text{--}1.3$  eV, and the electron transfer from various arene donors to  $\text{NO}^+$  clearly falls into Class III (see eq 6). The striking feature of the resulting potential-energy surface (cross-section) in Figure 5<sup>42</sup> is the existence of the broad *single minimum* (compare the shape of curve d in Figure 4),<sup>47</sup> and the intermolecular complex is therefore designated as  $[\text{ArH}, \text{NO}]^+$  with the charge placed *outside* the brackets to emphasize the existence of only one potential well on the pathway between the  $(\text{ArH} + \text{NO}^+)$  reactants and the  $(\text{ArH}^+ + \text{NO}^*)$  products. Intermolecular

electron-transfer reactions that belong to the *Class III* category with:  $H_{\text{DA}} > \lambda_{\text{CE}}/2$  occur with no activation barrier.

**B. Potential-Energy Diagram for Arene Interaction with  $\text{NO}_2^+$  via Electron Transfer.** Owing to the very rapid thermal nitration of benzene and related arenes with  $\text{NO}_2^+$ , reliable spectrophotometric data on the charge-transfer interaction are not yet available<sup>48</sup> for the evaluation of the electronic coupling element in these systems. Nonetheless, to follow through with its comparison to  $\text{NO}^+$  (eq 5), let us consider the corresponding electron-transfer process, i.e., eq 8



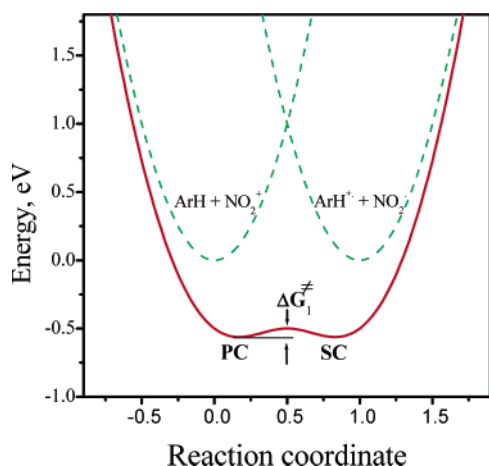
and initially rely on the comparison of the physical constants in Chart 1 to envisage some broad estimates of the electronic coupling element for the preequilibrium interaction in eq 8. We then proceed from the reorganization energy of the self-exchange:  $(\text{NO}_2^+ \rightleftharpoons \text{NO}_2^*)$  as:  $\lambda_{\text{NO}_2} = 140$  kcal/mol which is known to be roughly two times larger than  $\lambda_{\text{NO}}$ ;<sup>11b</sup> and we construct the adiabatic potential-energy surface for the  $\text{ArH}/\text{NO}_2^+$  dyad shown as the cross-section in Figure 6, based on the value of the electronic coupling element ( $H_{\text{DA}} = 1.7$  eV) estimated from the MO-calculated degree of charge-transfer ( $Z = 0.71$ ) in Table 1.<sup>40c</sup>

The increased reorganization energy for the cross exchange between  $\text{ArH}$  and  $\text{NO}_2^+$  in eq 8 with:  $\lambda_{\text{CE}} = 3.9\text{--}4.1$  eV places the  $\text{C}_6\text{H}_6/\text{NO}_2^+$  system in the Class II category (see eq 7); and this is seen in Figure 6<sup>42</sup> by the potential-energy diagram consisting of a double minimum (compare the shape of curve c in Figure 4) which replaces the single minimum characteristic of the  $\text{ArH}/\text{NO}^+$  system in Figure 5. This double potential-energy well consists of a separate *precursor*  $\pi$ -complex  $[\text{ArH}, \text{NO}_2^+]_{\text{PC}}$  and a *successor*  $\pi$ -complex  $[\text{ArH}^+, \text{NO}_2^*]_{\text{SC}}$  both with progressively shallower minima as the electronic coupling element  $H_{\text{DA}}$  decreases. In other words, as a result of the large

(47) For the Class III systems with:  $H_{\text{DA}} > \lambda_{\text{CE}}/2$ , the analytical expression for the adiabatic ground-state energy  $E_{\text{GS}}$  (as given in footnote 38) yields the single broad minimum shown.

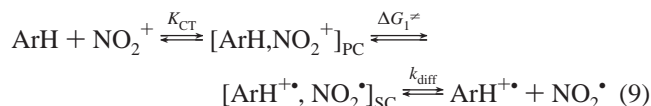
(48) (a) Preliminary studies indicate that it may be possible (at very low temperatures) to isolate the  $\sigma$ -complex of nitronium ( $\text{NO}_2^+$ ) similar to that obtained with bromonium ( $\text{Br}^+$ ) in ref 26. (b) Compare: Olah, G. A.; Lin, H. C.; Forsyth, D. A. *J. Am. Chem. Soc.* **1974**, *96*, 6908.

(46) (a) Ebersson, L. *Electron-Transfer Reactions in Organic Chemistry*; Springer-Verlag: New York, 1987; p 106. (b) Ebersson, L.; Gonzales-Lugue, R.; Lorentzon, J.; Merchan, H.; Roos, B. O. *J. Am. Chem. Soc.* **1993**, *115*, 2898.



**Figure 6.** Profile of the potential-energy surface (double minima) for  $\text{NO}_2^+/\text{ArH}$  dyads. The initial (reactant) diabatic state and final (product) diabatic state are quantitatively drawn (in green) to scale for  $\Delta G_{\text{ET}}^0 = 0.42$  and  $\lambda = 4.0$  eV in the dashed (left) and (right) curves, respectively. The adiabatic (red) curve shows the potential-energy surface calculated for  $H_{\text{DA}} = 1.7$  eV in benzene nitration with  $\text{PC} = [\text{ArH}, \text{NO}_2^+]$  and  $\text{SC} = [\text{ArH}^+, \text{NO}_2^*]$ , and the activation energy  $\Delta G_1^\ddagger \approx 0.5$  kcal mol $^{-1}$ .

reorganization energy of  $\text{NO}_2^+$ , its intermolecular interaction with  $\text{ArH}$  cannot progress via a single  $\pi$ -complex like that with  $\text{NO}^+$ , but includes a pair of the  $\pi$ -electronic isomers (electromers) in eq 9.<sup>49</sup>



Thus, the transient PC and SC complexes in Figure 6 are separated by the rate-limiting barrier ( $\Delta G_1^\ddagger$ ) that becomes progressively higher as the electronic interaction between the  $\text{ArH}/\text{NO}_2^+$  moieties decreases. The subsequent diffusive separation ( $k_{\text{diff}}$ ) completes the overall electron transfer in eq 9.

## Discussion

The mechanistic strategy in this study is first based on: (A) experimentally establishing the reactive intermediates in the electrophilic reaction of arenes with  $\text{NO}^+$  in the rather slow aromatic nitrosation process, (B) developing an *independent* theoretical methodology to map out the potential-energy surface by ab initio quantum mechanics, and (C) simultaneously analyzing the pertinent electronic interactions of arenes with  $\text{NO}^+$  by the application of Marcus–Hush theory. Upon the successful melding of (A), (B), and (C), this conceptual process is then reversed and the theoretical treatments (B) and (C) are used to theoretically deduce (A) the reactive intermediates in the very fast electrophilic reaction of arenes with  $\text{NO}_2^+$  to form a coherent mechanism for aromatic nitration as follows.

(49) (a) Although there is extensive electron delocalization in both the precursor and successor complexes in eq 9, the charges are written inside (and not outside) the brackets to emphasize their individuality as separate PC and SC complexes. (b) In eq 9, the electron-pair redistribution from the arene donor<sup>35</sup> (HOMO) attendant upon the formation of the PC with  $Z = 0.7$  (equivalent to  $c_b^2 = 0.35$ ) corresponds to the overall transfer of 0.7e to the  $\text{NO}_2^+$  acceptor (LUMO) with 1.3e retaining the character of the arene HOMO. (c) Since the (PC  $\rightarrow$  SC) transformation arises as a result of 1-electron transfer from the arene-centered orbital to a  $\text{NO}_2$ -centered orbital, the resultant 2-electron distribution in the SC becomes 1.0e on the  $\text{NO}_2^+$  moiety with 1.0e remaining on the  $\text{ArH}$  moiety. As a result, the SC takes on the chemical character of a radical pair (i.e.,  $\text{ArH}^+/\text{NO}_2^*$ ) which is conducive to bond formation and thus facilitates the formation of the  $\sigma$ -adduct in eq 11.

**I. Conciliation of the Molecular-Orbital and the Marcus–Hush Potential-Energy Surfaces for Aromatic Nitrosation and Nitration. A. Mechanism of Electrophilic Nitrosation—One Reactive Intermediate.** The thorough search of the potential-energy surface by ab initio electronic structure calculations of the  $\text{C}_6\text{H}_6/\text{NO}^+$  pair reveals the existence of only a single minimum.<sup>50</sup> Likewise, the spectral (charge-transfer) detection and complete structural/electronic characterization with the aid of Marcus–Hush theory identify the unusual  $\pi$ -complex  $[\text{Ar}, \text{NO}]^+$  as the critical intermediate which is further subject to electron-transfer according to eq 5. This energy well lies at  $-36$  kcal mol $^{-1}$  below the diabatic reactants state and is formed prior to the product, N-protonated nitrosobenzene, which lies at  $-42$  kcal mol $^{-1}$  (Figure 1B). The optimized  $\pi$ -structure of this reactive intermediate can be compared with those isolated earlier as crystalline salts and structurally characterized by X-ray crystallography. Indeed, Table 1 shows that the structural parameters of the  $\pi$ -complexes obtained by molecular-orbital and X-ray determinations are essentially identical; and the predicted coincidence of the intermolecular separation parameter  $r_{\text{DA}}$  (which is especially difficult to calculate reliably) is most noteworthy. The latter together with the high (calculated and measured) degree of charge transfer in Table 1 underscores the unusually strong charge-transfer forces with large values of  $H_{\text{DA}}$  that bind the  $\text{ArH}/\text{NO}^+$  moieties in the intermolecular complex. Thus at the energy minimum of the  $\pi$ -complex, the reaction coordinates of the molecular-orbital (MO) surface and the Marcus–Hush surface are essentially superimposable in this region.

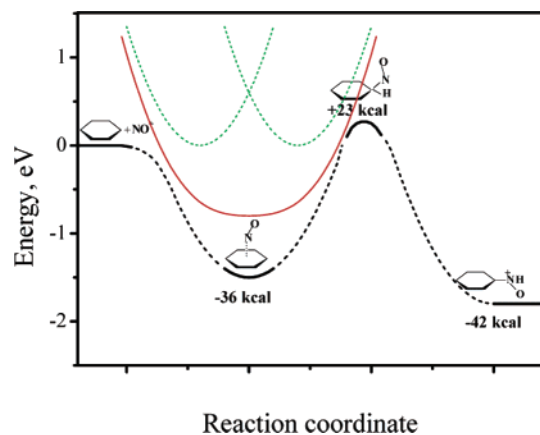
The further scrutiny of the MO-based potential-energy surface following the intermolecular  $\pi$ -complex reveals no other minima along the reaction coordinate prior to the nitrosated product, but a single (strong) maximum is detected in an intermediate region at  $+23$  kcal mol $^{-1}$ . To complete the mechanistic formulation of aromatic nitrosation, we identify the structure illustrated in Figure 3A (not associated with any other near local minima) to be a close approximation to the transition-state structure.<sup>51</sup> Because the Marcus–Hush surface diverges from the molecular-orbital surface beyond the  $\pi$ -complex, electron-transfer provides only limited insight of the ensuing transition state.

It is noteworthy that the MO-based potential-energy surface schematically presented in Figure 7 bears the general topological features of the conventional mechanism of electrophilic aromatic substitution, with the one important exception being the absence of the Wheland intermediate.<sup>52</sup> The acceptance of the electron transfer (eq 5), leads to the slow step in aromatic nitrosation which is largely represented by the homolytic dissociation of

(50) Although three other substantially higher-lying minima (probably accessed in the initial reactants encounter) were located, we expect their facile collapse to the stable  $\pi$ -complex owing to very low barriers and high exergonicities.

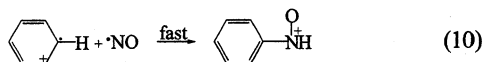
(51) The transient structure in Figure 3A is from MP2/6-31G\* calculations and will be further elaborated at the higher level of theory involving precise CCSD(T) optimizations.

(52) (a) See, for example: the qualitative reaction diagrams in the textbook references cited in footnote 1. Strictly speaking however, whether the Wheland structure is a transition state or a high-energy intermediate<sup>54a</sup> does not materially affect this mechanistic formulation. (b) For the quantitative comparison of Figure 7 with aromatic nitrosation in solution, a minor energy adjustment for solvation (especially between the diabatic products state and the other stationary points) must be made, as described in the footnotes 63 and 64. Moreover, the energy of the diabatic reactant state ( $\text{ArH} + \text{NO}^+$ ) in Figure 7 must also be lowered by an extra amount described in footnote 63a.



**Figure 7.** Potential-energy diagram for electrophilic aromatic nitrosation (black). The schematic representation (not drawn in scale) is based on the ab initio molecular-orbital (search) methodology described in the text. The graphic relationship of the molecular-orbital surface to the Marcus–Hush surface (red) derives from the juxtaposition of the interacting diabatic reactants/final states:  $[\text{ArH} + \text{NO}^+]/[\text{ArH}^{+\bullet} + \text{NO}]$  in green from Figure 5.<sup>64a</sup>

the intermolecular  $\pi$ -complex; (designated as  $K_{\text{et}}$  in eq 5).<sup>53</sup> As such, the rate-limiting transition state is traversed during the rapid bimolecular coupling<sup>53</sup> of  $\text{ArH}^{+\bullet}$  and  $\text{NO}^{\bullet}$  with concomitant breaking of the carbon–hydrogen bond. This process is tantamount to the direct insertion of  $\text{NO}^{\bullet}$ , e.g.<sup>54,55</sup>



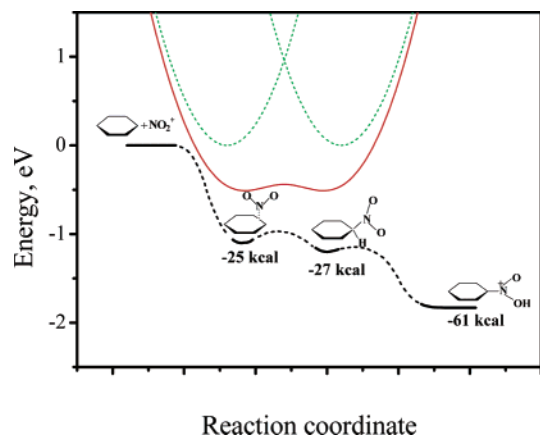
for which we are unaware of any precedence,<sup>54</sup> but it is roughly akin to that proposed earlier by Skokov and Wheeler.<sup>19</sup> On the basis of this mechanism, slow rates of aromatic nitrosation are readily attributed to the homolytic dissociation of the intermolecular complexes, ( $-\Delta G_{\text{ET}}$ ), which is highly endergonic for most aromatic donors, with the exception of the very electron-rich ones such as phenols and anilines.

**B. Mechanism of Aromatic Nitration—Two Critical Intermediates.** Our success with the molecular-orbital methodol-

(53) (a) The charge-transfer formulation of aromatic nitrosation is thus best described as the combination of eq 5 plus eq 10. (b) At this juncture, there is ambiguity as to the stage or “separation” state at which the homolytic coupling of the ion-radical pair effectively occurs. Because this must be closer than that of the thermodynamically free (paramagnetic) pair, the value of  $\Delta G_{\text{ET}}$  represents the maximum (activation) barrier, provided reversibility is not included. However, some degree of the latter may have to be included to accommodate the observed deuterium kinetic isotope effects, because they are minimal in the preequilibrium steps in eq 5.

(54) (a) However, for the analogous behavior of the CT (photo)generated radical pair:  $\text{ArH}^{+\bullet}/\text{NO}^{\bullet}$ , see: Hubig, S. M.; Kochi, J. K. *J. Am. Chem. Soc.* **2000**, *122*, 8279. (b) The fast insertion process can be schematically represented as eq 10, in which coupling is synchronous with hydrogen migration. As such, the  $\sigma$ -complex or classical Wheland structure<sup>57</sup> is not an intermediate, but lies close to the transition state in CCSD(T) optimizations. Interestingly, the insertion in eq 10 is related to the organometallic process with carbonylmetal(0) donors recently described by Melenkivitz, R.; Southern, J. S.; Hillhouse, G. L.; Concolino, T. E.; Liable-Sands, L. M.; Rheingold, A. L. *J. Am. Chem. Soc.* **2002**, *124*, 12 068. (b) The aromatic cation radicals and free(uncomplexed)  $\text{NO}^{\bullet}$  that are commonly observed as byproducts when arene donors and  $\text{NO}^+$  interact, then result from the competition between coupling in eq 10 and diffusive separation.<sup>55</sup> (c) The nitrous-acid catalysis of aromatic nitration (and particularly the CIDNP results of Ridd et al.) have important bearing directly on this point (see the discussion by Olah et al. in ref 65, pp 129 ff.

(55) (a) In their calculation, Peluso et al.<sup>25</sup> also describe the (probable) formation of a  $\pi$ -complex as a charge-transfer ( $\text{ArH}^{+\bullet} + \text{NO}_2^{\bullet}$ ) state that leads to homolytic dissociation similar to the gas-phase behavior observed by: (b) Schmitt, R. J.; Buttrill, S. E. Jr.; Ross, D. S. *J. Am. Chem. Soc.* **1984**, *106*, 626. (c) Morrison, J. D.; Stenney, K.; Tedder, J. M. *J. Chem. Soc. Perkin Trans. 2* **1981**, 967. (d) Attina, M.; Cacace, F.; Yanez, M. *J. Am. Chem. Soc.* **1987**, *109*, 5092. (e) Attina, M.; Cacace, F. *Gazz. Chim. Ital.* **1988**, *118*, 241.



**Figure 8.** Schematic representation of the potential-energy diagram for electrophilic aromatic nitration (black) as based on the ab initio molecular-orbital calculations described in the text. The graphic relationship of the molecular-orbital surface to the Marcus–Hush surface (red) derives from the superposition of the  $\pi$ - and  $\sigma$ -complexes with the PC and SC complexes  $[\text{ArH}, \text{NO}_2^+]$  and  $[\text{ArH}^{+\bullet}, \text{NO}_2^{\bullet}]$ , respectively, from Figure 6.<sup>64b</sup>

ogy in accurately reproducing the potential-energy surface for  $\text{NO}^+$  allows us the confidence to now extend it to  $\text{NO}_2^+$ , for which pertinent experimental data are otherwise unavailable. By the same search procedure, we rigorously explore the potential-energy surface by ab initio electronic structure calculations for intermolecular interactions of the  $\text{C}_6\text{H}_6/\text{NO}_2^+$  pair. Most importantly, this procedure reveals the existence of a pair of close lying minima at  $-25$  and  $-27$  kcal mol<sup>-1</sup> below the diabatic reactants state of ( $\text{C}_6\text{H}_6 + \text{NO}_2^+$ ), as shown in Figure 8, which bears a strong resemblance (but is not identical) to the adiabatic electron-transfer surfaces developed in Figure 6 from Marcus–Hush theory. In both cases, the principal features consist of double potential-energy wells as follows:<sup>42</sup>

(i) The first potential-energy minimum is clearly identified as the intermolecular  $\pi$ -complex because the  $\text{NO}_2^+$  moiety lies directly atop the benzene rim.<sup>56</sup> The (noncovalently bonded) separation of 2.175 Å is strongly reminiscent of that (2.115 Å) in the corresponding  $\pi$ -complex of benzene and  $\text{NO}^+$ , as described in Table 1. Most significant is the bending of the linear  $\text{NO}_2^+$  to an O–N–O angle of  $2\theta = 141^\circ$  in Figure 2A; and such a sizable angular contraction indicates that the  $\text{NO}_2^+$  moiety undergoes effectively an (almost) complete reduction to  $\text{NO}_2^{\bullet}$  ( $2\theta = 134^\circ$ ) upon arene complexation. The latter coincides with the accompanying enlargement of the benzene moiety with the average C–C bond distance of 1.41 Å close to that in the benzene cation radical.<sup>56</sup> It is important to note that the degree of charge transfer of  $Z = 0.71$  in the  $\pi$ - $[\text{C}_6\text{H}_6, \text{NO}_2]^+$  complex calculated from the Mulliken population analysis of the electron-density distribution is essentially indistinguishable from that extant in the  $\pi$ -complex of benzene and  $\text{NO}^+$  in Table 1. [Like the latter, placement of the positive charge outside the brackets signifies extensive intermolecular charge (electron) delocalization].

The electronic structure of such a  $\pi$ -complex on the Marcus–Hush surface is similarly described as a strong charge-transfer (precursor) complex designated as  $[\text{ArH}, \text{NO}_2^+]_{\text{PC}}$  in eq 9, and involving extensive charge (electron) redistribution between the

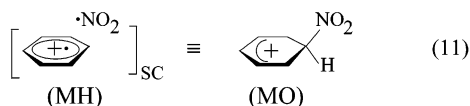
(56) For the precise bond distance/angle parameters of this and other structures in Figures 1–3 calculated via the coupled-cluster CCSD(T) optimizations, see the coordinates listed in the Supplementary Information Available.



arene donor and  $\text{NO}_2^+$ . Moreover, the MO-calculated degree of charge-transfer of  $Z = 0.71$  translates to the electronic coupling element of  $H_{\text{DA}} = 1.7$  eV.<sup>40</sup> Such significant values of the electronic coupling element are more than sufficient to offset the reorganization energy penalty for the O–N–O bending that accompanies the spontaneous formation of the  $\pi$ -complex. As a result, this  $H_{\text{DA}}$  value leads to the potential-energy surface shown as the cross section (red) in Figure 6 for adiabatic electron transfer between the ArH and  $\text{NO}_2^+$  according to eq 9. The coincidence of the molecular-orbital-based structure of the  $\pi$ -complex (Figure 2A) with the Marcus–Hush-based precursor complex  $[\text{ArH}, \text{NO}_2^+]_{\text{PC}}$  indicates that the reaction coordinate of the aromatic nitration and the electron transfer are essentially superimposable in this region, much like that designated for the  $\pi$ -complex  $[\text{ArH}, \text{NO}^+]$  in aromatic nitrosation (vide supra).

(ii) The further traverse along the  $\text{C}_6\text{H}_6/\text{NO}_2^+$  surface reveals an isomeric intermediate (see Figure 8) at almost the same energy as the  $\pi$ -complex. In this second species, the direct attachment of the  $\text{NO}_2^+$  moiety to the benzene ring at the covalent (C– $\text{NO}_2$ ) distance of 1.55 Å approximates that (1.47 Å) in nitrobenzene itself, and the tetrahedral character of this ipso-carbon center indicates a  $\sigma$ -bonded intermediate (Figure 3B). Indeed, the detailed comparison of its structural features in Table 2 with those of related  $\sigma$ -complexes of various arenes (previously established by X-ray crystallography)<sup>57</sup> confirm this as the Wheland intermediate in aromatic nitration.

On the other hand, the second minimum on the Marcus–Hush surface is the successor complex in adiabatic electron transfer designated as  $[\text{ArH}^{+\bullet}, \text{NO}_2^*]_{\text{SC}}$  in eq 9. To obtain a coherent picture of the second minima found as the  $\sigma$ -complex and the successor complex, let us proceed as follows. First, the coincidence of the molecular-orbital and the Marcus–Hush reaction coordinates in the region around the  $\pi$ -complexes (vide supra) allows us to superpose the Marcus–Hush profiles (Figures 5 and 6) onto the molecular-orbital surfaces as shown in Figures 7 and 8. Having established this juxtaposition around the first minima, the second minima on the molecular-orbital (MO) and Marcus–Hush (MH) surfaces in aromatic nitration are then strongly correlated in energy; and we believe they are also rather closely juxtaposed structurally according to eq 11 such that essentially no energy barrier separates the two.<sup>49b,58</sup>



Indeed, the facile collapse<sup>59</sup> of the Mulliken–Hush structure to the molecular-orbital structure is analogous to that designated for the homolytic coupling of  $\text{ArH}^{+\bullet}$  and  $\text{NO}^*$  (eq 10) in aromatic nitrosation. Most importantly, such a “barrierless” transformation is made possible by the absence of the significant reorganization

penalty, since the important (O–N–O) bending is already taken care of in the prior step involving the formation of the  $\pi$ -complex.

(iii) The last potential-energy minimum identified along the reaction coordinate is (protonated) nitrobenzene as the final product of aromatic nitration. Thus, the terminal step on the potential-energy surface involving the scission of the C–H bond in the  $\sigma$ -complex is fast and involves no deuterium kinetic isotope effect. The latter differs from the homolytic collapse (eq 10) of the ion-radical pair in nitrosation which (in the absence of the Wheland intermediate)<sup>54</sup> is accompanied by a simultaneous C–H cleavage and is subject to the (observed) kinetic-isotope effect.<sup>4b</sup> A thorough search reveals no other adducts (stable or otherwise) of  $\text{C}_6\text{H}_6$  and  $\text{NO}_2^+$ .

According to the electron-transfer mechanism in eq 9, the rate-limiting step occurs in the conversion of the precursor to the successor complex, and the activation barrier is evaluated as  $\Delta G_1^\ddagger = 0.5$  kcal mol<sup>-1</sup> based on the value of the electronic coupling element  $H_{\text{DA}} = 1.7$  eV as described by the potential-energy surface for adiabatic electron transfer (Figure 6).<sup>60</sup> Owing to eq 11, the same activation energy is predicted for the MO surface in Figure 8, which schematically presents the potential-energy diagram for aromatic nitration that includes the geminate intermediates (PC and SC), both as highly transient complexes. Most striking is the strongly divergent (gross) topology of the potential-energy diagram for aromatic nitrosation with  $\text{NO}^+$  in Figure 7 relative to that for aromatic nitration with  $\text{NO}_2^+$  in Figure 8. Thus even a cursory inspection clearly shows why aromatic nitrosation is so relatively slow and aromatic nitration so fast.<sup>61,62</sup>

**C. Effect of the Environment.** The ultimate conciliation of the ab initio quantum-mechanical with the Marcus–Hush (semiempirical) methodologies must take cognizance of the optimized molecular-orbital structures computed in vacuo relative to those evaluated from spectral measurements in solution. Since the present-day computational capabilities for solvent effects do not match those for structure determinations,<sup>8</sup> our treatment in Table S1 is rather simply based on the continuum solvation model using the B3LYP density functional, which we believe is sufficient to evaluate the principal changes in relative energies of various species. As a result of the strong emphasis on the electrostatic interaction in this model, let us (conceptually) replace the diabatic reactants state ( $\text{C}_6\text{H}_6$  plus  $\text{NO}^+$  or  $\text{NO}_2^+$ ) with the diabatic final state ( $\text{C}_6\text{H}_6^{+\bullet}$  plus  $\text{NO}^*$  or  $\text{NO}_2^*$ ) because the latter are (electrostatically) more akin to the corresponding stationary-point structures.<sup>63</sup> Viewed in this way, the results in Table S1 (shown as the differences in parentheses) reveal that the dielectric medium does not alter in any fundamental way the applicability of the molecular-orbital calculations to the Marcus–Hush results.<sup>64</sup>

(57) Hubig, S. M.; Kochi, J. K. *J. Org. Chem.* **2000**, *65*, 6807.

(58) (a) It is also important to note that the  $\sigma$ - and SC-structures are also correlated electronically, since the same electron-density shift from the ArH to  $\text{NO}_2^+$  moieties occurs in the  $\text{PC} \rightarrow \text{SC}$  (Marcus–Hush) and the  $\pi \rightarrow \sigma$  (molecular-orbital) transformations. (b) The latter as a least motion transformation probably proceeds without the intervention of “free”  $\text{ArH}^{+\bullet}/\text{NO}_2^*$  radicals (compare footnotes 53 and 54).

(59) For independent measurements of the very fast rates of homolytic coupling of related ion-radical pairs ( $\text{ArH}^{+\bullet} + \text{NO}_2^*$ ), see Figure 6 in Kim, E. K.; Bockman, M. T.; Kochi, J. K. *J. Am. Chem. Soc.* **1993**, *115*, 3103.

(60) Note that in Figure 6, The activation energy is:  $\Delta G_1^\ddagger = (\lambda_{\text{CE}} - 2H_{\text{DA}})^2/4\lambda_{\text{CE}} = 0.5$  kcal mol<sup>-1</sup>.

(61) (a) The cationic sigma complex is an energy minimum in nitration whereas it is (or lies close to) the transition state for nitrosation. (b) It is interesting to speculate that the ( $\pi \rightarrow \sigma$ ) transformation in nitration follows the principle of least motion,<sup>62</sup> whereas such a smooth transformation cannot occur with nitrosation. (c) For the quantitative comparison of the potential-energy diagram in Figure 8 with that applicable to aromatic nitration in solution, a minor energy adjustment for solvation (especially between the diabatic products state and the  $\pi$ - and  $\sigma$ -complexes) must be made, as described for aromatic nitrosation in footnote 52b.

(62) For the least motion in electrophilic aromatic substitution, see: Rosokha, S. V.; Kochi, J. K. *J. Org. Chem.* **2002**, *67*, 1727.

**II. Charge-Transfer Mechanism Relative to Earlier Studies of Electrophilic Aromatic Nitration.** The extensive literature on the various mechanistic aspects of electrophilic aromatic nitration, both experimental and theoretical, has been authoritatively reviewed by Olah, Malhotra, and Narang<sup>65</sup> (and the reader is strongly encouraged to consult this concise and well-balanced account). It is generally accepted that most if not all nitration mechanisms of ArH with NO<sub>2</sub><sup>+</sup> revolve around the putative Wheland or  $\sigma$ -complex as the critical (high-energy) intermediate, although it has hitherto eluded either isolation or structural and electronic characterization. To rationalize arene reactivity and selectivity, various types of preequilibrium intermediates have also been invoked in which, to quote Olah “.....The differences are a matter of degree. At one extreme we have the Schofield model in which the aromatic and the NO<sub>2</sub><sup>+</sup> ion have come together in an encounter complex, but they are not interacting. At the other extreme is Perrin’s suggestion in which the electron has been completely transferred to the NO<sub>2</sub><sup>+</sup> ion. Somewhere between is the  $\pi$ -complex suggested by Olah...”<sup>66a</sup> This insightful overview applies specifically to aromatic nitration and underscores the need to involve a second intermediate in addition to the  $\sigma$ -adduct (Wheland intermediate).

The charge-transfer mechanism as presented in eq 9 and Figure 8 is quantitative. First, the rigorous (quantum-mechanical) search methodology unambiguously identifies the potential-energy minima, and it structurally elucidates the  $\pi$ - and  $\sigma$ -complexes of arene (ArH) and NO<sub>2</sub><sup>+</sup>. Second, the electronic characterization of the  $\pi$ -complex derives from the firm theoretical basis of Mulliken charge transfer.<sup>36</sup> Third, the direct (inextricable) relationship between Mulliken charge transfer and classical electron transfer is established by Mulliken–Hush theory.<sup>37,67</sup> Fourth, the potential-energy surface independently developed by ab initio molecular-orbital calculations can be shown to coincide with that deduced from the semiquantitative treatment of Marcus–Hush electron transfer;<sup>58</sup> and Fifth, the preorganization of ArH and NO<sub>2</sub><sup>+</sup> as an unusual (CT)  $\pi$ -complex is merely one example of the more general (diffusion-controlled) association of electron donors and electron acceptors that have been extensively documented.<sup>68</sup>

Critical to the charge-transfer mechanism is the strong electronic coupling element  $H_{DA}$  in the [1:1] intermolecular association, that is *simultaneously* accompanied by extensive charge (electron) delocalization between the arene donor and

NO<sub>2</sub><sup>+</sup>. Three important mechanistic consequences follow from the rapid formation of such unusual (highly polarized)  $\pi$ -complexes as follows:

(1) Because the donor and acceptor components in the  $\pi$ -complex are structurally akin to the aromatic cation radical (ArH<sup>•+</sup>) and nitrogen dioxide (NO<sub>2</sub><sup>•</sup>), respectively, the usual reorganization penalty ( $\lambda_{NO_2}$ , pathway associated with the O–N–O bending), is offset by the strong electronic coupling ( $H_{DA}$ ) and does not explicitly contribute to the reaction dynamics.<sup>69</sup> As a result, the principal activation barrier lies between the  $\pi$ - and  $\sigma$ -complexes ( $\Delta G_1^\ddagger$  in Figure 6); and this is severely truncated by increasing values of  $H_{DA}$ . In other words, the *driving force for overall electron transfer* ( $-\Delta G_{ET}$ ) is *not necessarily a major factor in the overall kinetics for aromatic nitration*.<sup>70</sup> A corollary to this conclusion is that the classical (Wheland)  $\sigma$ -structure is not necessarily the critical (high-energy) intermediate along the reaction coordinate, as commonly formulated.<sup>1–3, 65, 69</sup>

(2) Reactivity and selectivity are established in separate steps—the arene activation being a factor in  $\pi$ -complex formation (which is driven by redox thermodynamics), and positional selectivity being established in the subsequent collapse of the  $\pi$ -complex (which is largely determined by the spin-density distribution inherent to the cation-radical character in the arene moiety<sup>71</sup>). The precursor and successor complexes in eq 9 then correspond in Figure 8 to the separate  $\pi$ - and  $\sigma$ -complexes, respectively, as advocated by Olah et al.<sup>66b</sup> Indeed, the double potential-energy minima coupled with the low barrier (Figure 8) provide the obvious explanation as to how aromatic nitration with NO<sub>2</sub><sup>+</sup> can be very fast (encounter-controlled) and yet maintain high positional selectivity.<sup>68d</sup>

(3) Although paramagnetic character is strongly induced in both the arene and NO<sub>2</sub><sup>+</sup> moieties during  $\pi$ -complex formation, *free radicals* (or ion-radicals) as easily diffusing paramagnetic entities are not important intermediates [except to an extent to which one or more separate (diffusional) processes can compete].<sup>72</sup>

Taken all together, we posit that these important facets of the charge-transfer mechanism allow the hitherto disparate

- (63) (a) This comparison owes to the large disparity in the ionic radii of the small cations (NO<sup>+</sup> and NO<sub>2</sub><sup>+</sup>) compared to those of the relatively large arene donors, since the size bears a reciprocal-radius relationship to the solvation energy. Therefore it is primarily the diabatic reactants state (ArH + NO<sup>+</sup>) that must primarily be corrected for solvation.<sup>64</sup> (b) Similarly, the spectroscopic properties of the various intermolecular complexes are not (very) solvent dependent since the values of  $\nu_{CT}$  measured in dichloromethane are not fundamentally different from those in acetonitrile.<sup>37</sup> (c) For the experimental evaluation of solvation, we judge that:  $E_{red}^\circ \approx 2$  V vs SCE in the gas phase, based on the extrapolation of the observed difference of:  $\Delta E_{red}^\circ = 0.2$  V in dichloromethane and acetonitrile.<sup>63d</sup> (d) Lee, K. Y.; Kuchynka, D. J.; Kochi, J. K. *Inorg. Chem.* **1990**, *29*, 4196.
- (64) (a) For the direct application of the MO-based potential-energy surface in Figure 7 to the aromatic nitrosation process, the diabatic reactants [C<sub>6</sub>H<sub>6</sub> + NO<sup>+</sup>] state must be lowered by roughly 12 kcal mol<sup>-1</sup> in dichloromethane and 16 kcal mol<sup>-1</sup> in acetonitrile.<sup>63a, c</sup> (b) A similar correction for solvation should be carried out for [C<sub>6</sub>H<sub>6</sub> + NO<sub>2</sub><sup>+</sup>] in Figure 8 as a comparison to aromatic nitration. (c) We hope that further (theoretical) studies will more fully quantify the effects of the solvation on the potential-energy diagrams.
- (65) Olah, G. A., Malhotra, R., Narang, S. C. *Nitration: Methods and Mechanisms*; VCH: New York, 1989.
- (66) (a) The quotation is from Olah et al. in ref 65, p 166. (b) Olah’s requirement for and description of two (separate) intermediates in aromatic nitration are clearly presented on pp 134 ff.
- (67) For an early attempt, see: Fukuzumi, S.; Kochi, J. K. *J. Am. Chem. Soc.* **1980**, *102*, 2928.

- (68) (a) Foster, R. *Organic Charge-Transfer Complexes*; Academic: New York, 1969. (b) Briegleb, G. *Electronen-Donator-Acceptor Komplexe*; Springer: Berlin, 1961. (c) Andrews, L. J.; Keefer, R. M. *Molecular Complexes in Organic Chemistry*; Holden-Day: San-Francisco, 1964. (d) For the recent update on aromatic donors, see: Rosokha S.; Kochi, J. K. In *Modern Arene Chemistry*; Astruc, D., Ed.; VCH–Wiley: New York, 2002 (chapter 13), pp 435 ff.
- (69) Because the electronic coupling element ( $H_{DA}$ ) depends on both the arene donor as well as the NO<sub>2</sub><sup>+</sup> acceptor, the magnitude of  $H_{DA}$  could vary markedly in the general formulation of aromatic nitration with other “nitronium” carriers.<sup>69c</sup> In the limit of very small  $H_{DA}$  (<200 cm<sup>-1</sup>), the potential-energy surface will take on the characteristics of the Marcus outer-sphere mechanism,<sup>44</sup> and the overall driving force for electron transfer could affect the kinetics. Furthermore, with decreasing magnitudes of  $H_{DA}$ , the potential-energy diagrams increasingly take on a more traditional character, with the high-energy  $\sigma$ -complex approaching the rate-limiting transition state. (b) It is particularly important to note that despite such differences in  $H_{DA}$  of NO<sub>2</sub><sup>+</sup> versus that of various N-nitropyridinium acceptors, the selectivities are remarkably invariant,<sup>69c</sup> and this points to the occurrence of common intermediates. (c) Kim, E. K.; Lee, K. Y.; Kochi, J. K. *J. Am. Chem. Soc.* **1992**, *114*, 1756.
- (70) For the other (nonisergonic) electron-transfer processes, the cross-sectional shapes of the potential-energy surfaces will differ from those in Figures 4–6 consonant with the magnitudes of the driving force ( $-\Delta G_{ET}$ ). Nonetheless, strong donor/acceptor interactions in such systems will persist and also result in the following: (i) lowering the electron-transfer barrier and (ii) substantial stabilization of the PC and SC relative to the diabatic states.<sup>36b, c</sup> as illustrated in Figure S1 in Supporting Information.
- (71) Fukuzumi, S.; Kochi, J. K. *J. Am. Chem. Soc.* **1981**, *103*, 7240, and references therein.
- (72) Compare the gas-phase studies in ref 55b–d.

observations<sup>66a</sup> to be woven into a single coherent mechanism for aromatic nitration.

### Summary and Conclusion

The convergence of high level (ab initio) molecular-orbital calculations and the semiquantitative application of Marcus–Hush theory with experiment leads to the charge-transfer mechanism of electrophilic aromatic nitrosation and nitration; and this mechanistic formulation naturally accounts for the wide disparity that exists between the reactivity of  $\text{NO}^+$  and  $\text{NO}_2^+$  toward arene donors, despite their quite similar physical (and redox) properties as electrophiles.

Critical to the charge-transfer mechanism is the spontaneous (rapid) formation of intermolecular [1:1] complexes. In the case of  $\text{NO}^+$  and  $\text{NO}_2^+$ , the large magnitudes of the electronic coupling elements with various arene donors of  $H_{\text{DA}} \approx 1.5$  eV indicate the existence of strong intermolecular polarization (between ArH with  $\text{NO}^+$  and  $\text{NO}_2^+$ ) sufficient to ensure (almost) complete electron transfer concomitant with complex formation. However, as the result of a substantially larger reorganization energy of the triatomic  $\text{NO}_2^+$  relative to the diatomic  $\text{NO}^+$  (owing to bending), the Marcus–Hush potential-energy surface consists of a double minimum rather than the single minimum, and *independent* molecular-orbital calculations (Figure 8) afford detailed molecular structures of the relevant  $\pi$ - and  $\sigma$ -complexes in Figures 1–3. As such, the unusual molecular parameters, particularly of the  $\pi$ -complexes, provide unambiguous quantitative support for the importance of Mulliken charge-transfer to aromatic nitrosation and nitration.<sup>70</sup>

Finally, it is important to restate the (obvious) caveat that the MO-based energetics in Figures 7 and 8 must be quantitatively adjusted for solvation before they can be rigorously related to the nitration/nitrosation processes themselves. However, from

a mechanistic point of view, such a qualification is not limiting since the semiquantitative results in Table S1 indicate that the relative energies of the cationic (arene-containing) species are not strongly differentiated by the solvent dielectric. This important point is especially applicable to the close juxtaposition of the isomeric  $\pi$ - and  $\sigma$ -complexes (electromers) in the MO Figure 8 and the equivalent Marcus–Hush Figure 6. Indeed, the intimate (energetics) relationship between these  $\pi$ - and  $\sigma$ -complexes constitutes the distinctive core of the charge-transfer mechanism for electrophilic aromatic nitration with  $\text{NO}_2^+$  in solution.

**Acknowledgment.** S.V.R. and J.K.K. (Houston) thank the R.A. Welch Foundation and National Science Foundation for financial support. S.R.G. and M.H.-G. (Berkeley) were supported by a grant from the National Science Foundation (CHE – 9981997).

**Supporting Information Available:** Geometry optimizations and their implications for the reaction coordinate (pages S2–S3). CCSD(T) optimized structures for all stationary points reported in the paper (pages 4–7). A detailed breakdown of the total energies calculated at these stationary points (page 8). MP2 optimized structures for additional minima found for the [benzene, $\text{NO}$ ]<sup>+</sup> system (pages S9–S10), Table S1 on effects of the solvent dielectric on the relative stabilization energies based on the continuum solvent model (p.S11), and Figure S1 illustrating the effect of the electronic coupling element on the potential energy surface (cross-sections) for endergonic electron transfer (p.S12). This material is available free of charge via the Internet at <http://pubs.acs.org>.

JA021152S